CFD Modeling of Pump-Mix Action in Continuous Flow Stirred Tank

K. K. Singh and S. M. Mahajani
Dept. of Chemical Engineering, Indian Institute of Technology, Powai, Mumbai 400076, India

K. T. Shenoy and S. K. Ghosh
Chemical Engineering Div., Bhabha Atomic Research Centre, Trombay, Mumbai 400085, India

DOI 10.1002/aic.11349
Published online November 30, 2007 in Wiley InterScience (www.interscience.wiley.com).

The present work involves Computational Fluid Dynamics (CFD) modeling and validation of head and power characteristics of a Top Shrouded Turbine with Nonradial Rectangular Blades (TSTNRB) operated in backswept mode. Following the successful validation reported here and in two previous studies by the authors. CFD has been used to simulate the performance of different kinds of impellers viz. Straight Blade Paddle (SBP), Rushton Turbine (RT), Top Shrouded Turbine with Radial Rectangular Blades (TSTRRB), Top Shrouded Turbine with Radial Trapezoidal Blades (TSTRTB), Top Shrouded Turbine with Non-radial Rectangular Blades (TSTNRB), Top Shrouded Turbine with Curved Blades (TSTCB), and Both side Shrouded Turbine with Radial Trapezoidal Blades (BSTRTB), to compare them for pump-mix action. Baffle-impeller interaction has been modeled using the sliding mesh approach. Standard k-ε model has been used for turbulence modeling. The power number, head number, and flow number have been computed for each impeller. The impellers have been rated on the basis of head generated by them for equal specific power input. An attempt has been made to explain why different impellers operating at the same speed and handling the same inlet flow rate should give different heads. How this insight can be used to conceptualize better designs of pump-mix impeller is illustrated. © 2007 American Institute of Chemical Engineers *AIChE J,* 54: 42–55, 2008
Keywords: CFD, sliding mesh, pump-mix, power number, head number, flow number

Introduction

Because of certain inherent advantages like high stage efficiency, simplicity, and flexibility of operations, etc., mixer-settlers are widely used for solvent extraction which is an important unit operation. A cascade of mixer-settlers requires interstage, and at times, intrastage pumping of the phases being contacted. Instead of having separate pumps for this, pumping action of the impeller in the mixer itself can be harnessed to bring about this interstage or intrastage pumping of the process fluids. A mixer designed to serve this dual purpose of mixing and pumping is called a pump-mixer.[1,2] Pump-mixers are especially important in hydrometallurgical units where flow rates may be as high as a few hundred m^3/h and elimination of interstage pumps for such high flow rates is economically very attractive. Ideally speaking, phase separation in a settler is never complete as some drops of the dispersed phase are always entrained with the continuous phase. If pumps are used to transport this phase to the adjacent stage, the entrained drops, because of exposure to a very high shear in pumps, may further breakdown to give exces-

Correspondence concerning this article should be addressed to S. M. Mahajani at sanjaym@che.iitb.ac.in.

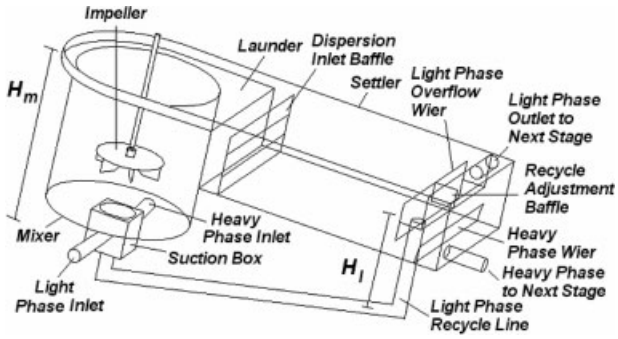

Figure 1. Schematic diagram of a single stage of pump-mix mixer settler with intra-stage recycle of light phase.

sively fine droplets. These excessively fine droplets may be too small to be recovered by the entrainment recovery plant and would, therefore, cause a permanent loss of the dispersed phase. Use of pump-mixers instead of pumps can preempt this possibility.

Since the purpose of the impeller in a pump-mixer is to provide both mixing and pumping, design an optimized pump-mixer information on both head and power characteristics of different impellers is required. Although numerous studies on mixers have been reported in the literature,[3–22] very few studies have been reported on pump-mixers.[23–28] Though, several commercial designs of pump-mixers like IMI design, Krebs design, Denevr design, Kemira design, Davy-Powergas design, and General Mills design have been reported in the open literature, only qualitative features have been discussed.[29,30]

Figure 1 shows the diagram of a pump-mix mixer settler with intrastage recycling of the light phase. For such a system, the duty of the pump-mix impeller is to meet the following requirements

$$a \leq \frac{P}{V} \leq b \tag{1}$$

$$h_r > \frac{\rho_m H_m - \rho_l H_l}{\rho_l} \tag{2}$$

Whereas, below the lower limit of specific power input the stage efficiency of the mixer will be poor because of improper mixing and small interfacial area, above the upper limit the drops produced in the mixer will be very small and require a large settler to settle which in turn will escalate the operating and capital costs. These limits are system specific and established through batch mixing and settling experiments in the laboratory. While designing a pump-mixer for a high flow rate, the major issue is to satisfy the requirement of head. As both power consumed and head generated by an impeller increase with speed, it is quite likely that reliance only on variation of speed to satisfy the head requirement may breach the upper limit on the specific power input. To meet the requirement of both head and power, two different approaches can be followed. First, by making geometric changes after having selected a particular type of impeller; second, by choosing one from several possible impeller types after having fixed the geometry. The geometric changes can be variation in impeller to tank diameter ratio, impeller off-bottom clearance, number of blades, blade width, blade length, and in extreme cases using two mixer in series instead of a single mixer. To satisfy the design constraints using the second approach, information on head and power characteristics of different impellers and the strategies to modify the design of a given impeller, so as to satisfy the head and power requirement, should be available with the designer.

Though CFD has been extensively applied to study batch mixers, its application to pump-mixers has been surprisingly rare. To the best of our knowledge, there exist only two published studies on CFD simulation of pump-mixers.[23,24] The first of these studies[23] was done for a pilot scale pump-mixer (0.270 m^3) employing a TSTRTB. Total 27 CFD simulations to understand the effect of impeller off-bottom clearance, blade width, number of blades, impeller diameter, flow rate and impeller speed on head and power characteristics were carried out. Two different approaches to simulate interaction between the rotating impeller and the stationary baffles—sliding mesh and multiple reference frame—were compared and the former was found to be better. Good agreement between the predictions of the CFD models and experimental values was observed.

The second study[24] was carried out on a bench-scale pump-mixer (0.011 m^3). Again a TSTRTB was used in the study. In addition to simulate for head and power, CFD based virtual tracer experiments were also conducted. Results of CFD simulations were validated with experimental data. Validation of virtual exit age distribution curves with experimental exit age distribution curves helped indirectly validate the CFD predicted velocity field inside the mixer. Compartment modeling of exit age distribution curves was also carried out and a plug flow vessel followed by two perfectly mixed vessels in series was found to be the best compartment model. Based on compartment modeling, it was argued that low clearance designs, which are often preferred to get high head, can cause phase instability and adversely affect the mass transfer efficiencies.

This article presents the CFD simulations and its validations for a TSTNRB operated in backswept mode in a tank same as the one used in the first CFD study mentioned earlier. Following the successful validations at two different scales for the same type of the impeller and at the same scale for two different types of impeller, the pump-mix behavior of different impellers has been simulated using CFD, without resorting to further experiments. The impellers have been rated for the head generated by them for the same specific power input. Wealth of information on local flow field resulting from CFD simulations has been used to explain the variation in the head generated by different impellers operating at the same speed and handling the same inlet flow rate. Based on this insight better designs of pump-mix impellers are proposed. It should, however, be noted that no local validation of CFD predicted flow field has been attempted and therefore the results based on local flow field values should be considered with caution.

Though the pump-mixers are essentially used for producing liquid–liquid dispersions, single phase characteristics are equally important as they can be used to predict two phase

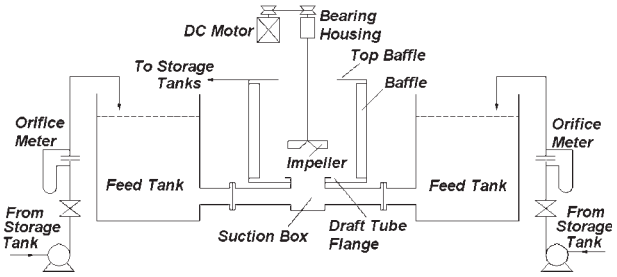

Figure 2. Schematic of experimental set-up.

behavior if suitably averaged physical properties are used.[31] Also, with the present state of computing resources, single-phase modeling serves as an indispensable first step to predict the quality of dispersion by solution of population balance models.[32–35]

CFD Simulations and Validation for TSTNRB

Experimental

The experimental set-up, shown in Figure 2, consists of a cylindrical tank of 0.7 m diameter and equal height. Four baffles, each of 0.65 m height, having width equal to 10% of tank diameter are provided to prevent vortex formation and enhance mixing. At the bottom plate of the tank is a suction orifice with diameter equal to ¼ of the tank diameter. The suction orifice provides connectivity between the tank and a cubical suction box (0.2 m side-length), which in turn is connected with two feed tanks. A flange is provided around the suction orifice to have the provision to mount a draft tube. Under steady state operation at a given flow rate, rotation of impeller causes suction of liquid from feed tank into the mixer from where it overflows back to the storage tanks. From storage tanks it is again pumped back to the feed tanks. Thus the system operates in a closed loop. The flow rates are maintained at desired values using valves and orifice meters located downstream of the pumps.

Several single-phase steady state closed loop experiments were conducted using water. For a given flow rate, level in the feed tank was measured both for stationary impeller and for impeller rotating at the desired speed. The difference in the two levels was recorded as the head developed by the impeller at that speed and flow rate. Power consumed by the impeller was measured by means of voltmeter and ammeter in the DC power supply line to the drive after deducting the losses and power consumed by the impeller in the dry runs. A TSTNRB, operated in backswept mode, was used in the study and is shown in Figure 3. The impeller diameter was half of the tank diameter, the disk thickness was 0.006 m, blade thickness was 0.005 m, hub outer diameter was 0.04 m, and hub height was 0.04 m. Hub inner diameter was 0.02 m to accommodate a shaft of the same diameter. Blade length was 0.17 m while the blade width was 0.07 m. The angle between the line joining the tip of the blade with the center and the blade was 10°. Experiments were performed for two off-bottom clearances (C/T = 0.3, 0.5). For each clearance, two flow rates were used (Q = 0.000556, 0.002222 m^3/s) and for each flow rate head and power were measured for four different impeller speeds (N = 2.275, 2.5, 2.733, 2.917 s^{-1}). Thus, total 16 experiments were conducted.

CFD simulations

CFD simulations, in this case, involve numerical solution of discretized equations - continuity equation for incompressible flow, Reynolds Averaged Navier-Stokes equations (RANS equations) and the equations of turbulence model. The equations are omitted here for brevity. Commercial CFD software FLUENT was used for the simulations. Sliding mesh technique was used to simulate interaction between the stationary baffles and the rotating impeller. Impellers in agitated tanks are known to generate large eddies and hence accurate local prediction of turbulent flow field would call for advanced but computationally expensive turbulence models such as large eddy simulation (LES). However, in the work reported here, wherein the CFD simulations have been used to predict macroscopic pump-mix characteristics, to reduce the computational requirement standard k-ε model has been used to model the turbulence. Adequacy of the standard k-ε model to predict the macroscopic performance parameters of pump-mix impellers has been demonstrated in two earlier studies.[23,24] SIMPLE algorithm was used for pressure–velocity coupling and second order upwind scheme was used for discretization of momentum and turbulence equations. For sliding mesh simulations, the interface separating the inner rotating volume surrounding the impeller and outer stationary volume surrounding the baffles was located midway between the impeller tip and baffle tip. Unstructured tetrahedral grids were used to discretize the computational domain. The grid size for the inner domain was 0.015 m while for the outer domain it was 0.025 m. Basis of the selection of grid size is discussed elsewhere.[23]

Figure 4 shows the details of the computational domain. For each converged CFD simulation, power consumption by the impeller was obtained by calculating the torque acting on the impeller blades as recommended in a previous study.[36] For each simulation, a steady state initial run was also carried out for stationary impeller but with the specified flow rate. The difference between outlet pressure and inlet pressure was recorded and the head was computed by subtracting this difference from the difference of outlet and inlet pressures obtained from the converged solution for the specified flow rate and the impeller speed.

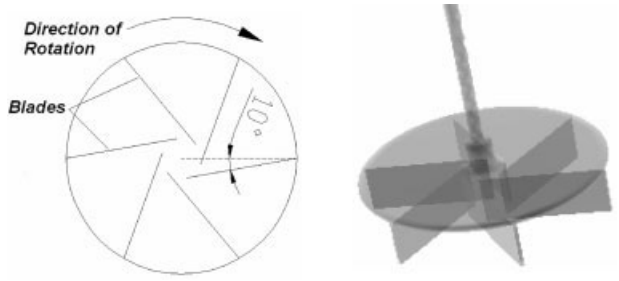

Figure 3. Top and 3-D view of the impeller (TSTNRB) used in the experiments.

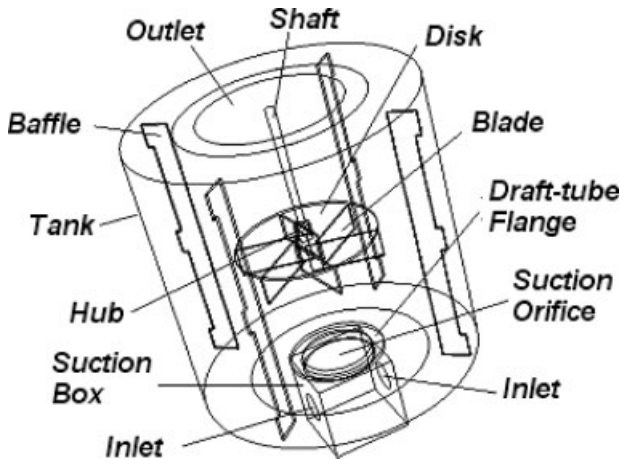

Figure 4. Computational domain.

Validation

Figures 5 and 6, respectively, show the parity plots for power consumption and head generated by the impeller for all the 16 runs. A good agreement between the CFD predictions and experimental values can be observed.

Comparison of Different Impellers for Pump-Mix Action

The three dimensionless numbers that help characterize the pump-mix action are the power number, the head number, and the pumping or flow number. These are defined as follows:

$$N_P = \frac{P}{\rho N^3 D^5} \tag{3}$$

$$N_H = \frac{gh}{N^2 D^2} \tag{4}$$

$$N_Q = \frac{Q_d}{ND^3} \tag{5}$$

A stirred tank employed as a pump-mixer is like a centrifugal pump with a large casing. The size of the casing is deliberately made large to ensure a finite residence time of the fluid. Owing to the large casing there is lot of internal recirculation. Thus, though the overall flow rate may be small the actual flow rate handled by the impeller is much more. The pumping number defined by Eq. 5 is based on the impeller discharge flow rate. Alternatively, another pumping number can be defined using the inlet flow rate. Using Eqs. 3 and 4, the head generated by the impeller for a given specific power input can be expressed as:

$$h = \left(\frac{\pi H T^2}{4\rho D^2 N_P}\right)^{2/3} \left(\frac{P}{V}\right)^{2/3} \frac{N_H}{g} \tag{6}$$

and the speed at which this head will be obtained can be given as:

$$N = \left(\frac{\pi H T^2}{4\rho D^5 N_P}\right)^{1/3} \left(\frac{P}{V}\right)^{1/3} \tag{7}$$

Therefore, for the same specific power input different impellers will give different heads because of their different head and power numbers. Knowledge of head and power numbers of different impellers is, therefore, important to identify the possible designs. The previous section shows the validation of CFD simulations for a TSTNRB operated in backswept mode. Following this and two earlier successful validation studies reported by the authors, CFD has been used to predict the head and power characteristics of different impellers without resorting to further experiments.

Figure 7 shows different types of impellers that are evaluated for the pump-mix action. These impellers are compared for a base case of inlet flow rate of 0.002222 m^3/s with $C/T = 0.3$, $D/T = 0.5$ in the tank geometry described in the experimental section. All the impellers have identical blade area. Both TSTNRB and TSTCB are evaluated for the operation in backswept (retreat blade) mode. For all the impellers, blade width is 0.07 m ($D/5$) unless otherwise mentioned in Table 1. For each impeller CFD simulations are carried out for four different speeds (N = 2.275, 2.5, 2.733 and 2.958 s^{-1}). Results from CFD simulations have been used to compute the power, head, and flow numbers. These are summarized in Table 1. The impellers are compared on the basis of the head generated by them for a given value of specific power input (P/V = 1000 W/m^3). The impeller speed at

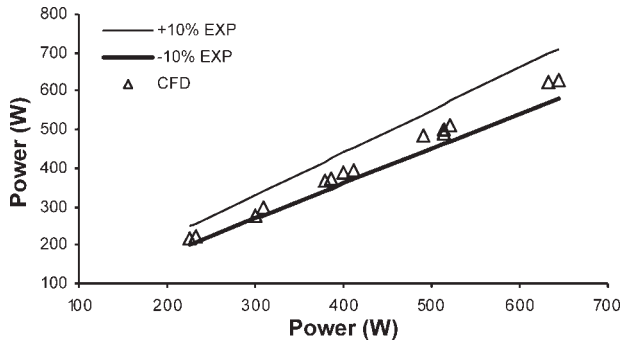

Figure 5. Parity plot for power predicted by CFD simulations.

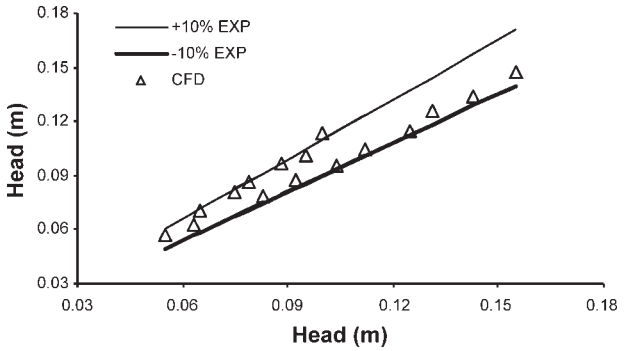

Figure 6. Parity plot for head predicted by CFD simulations.

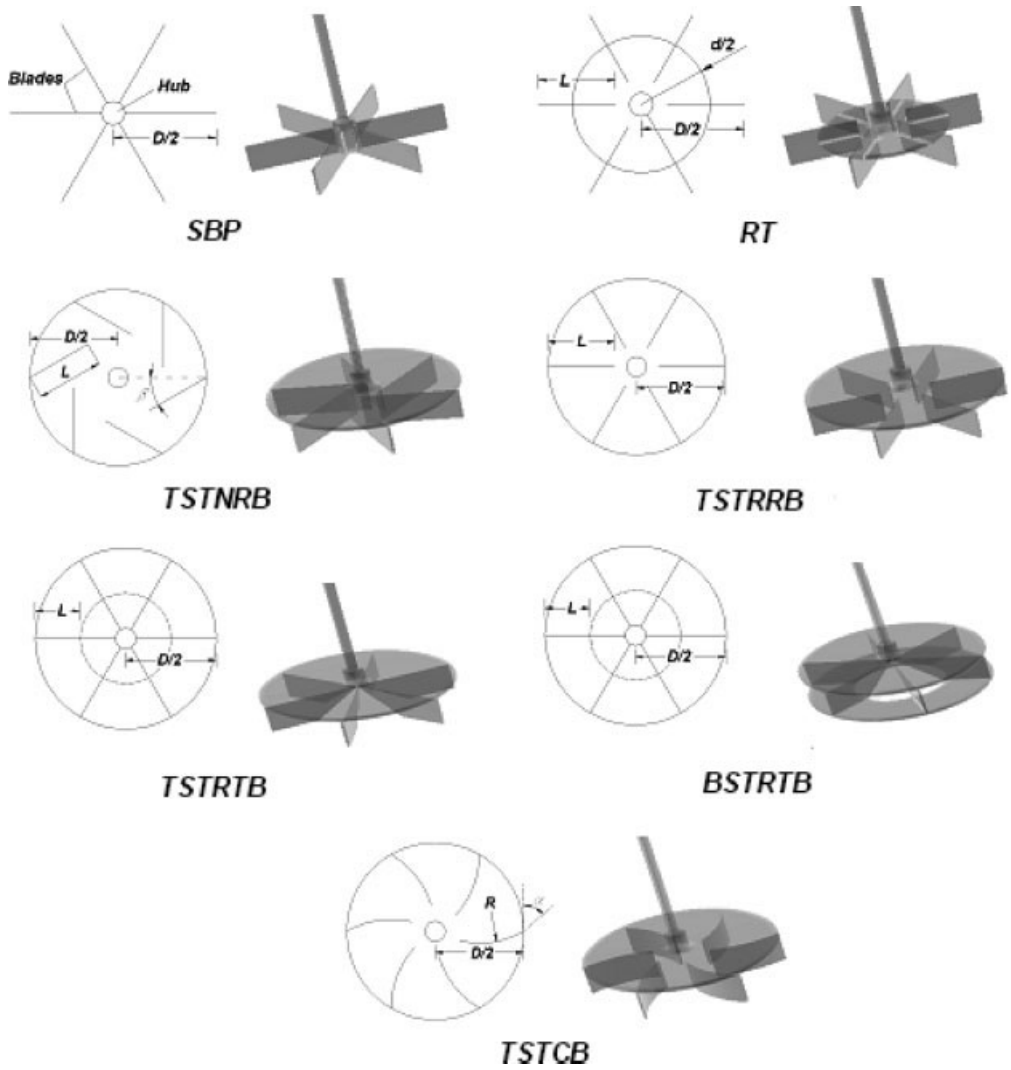

Figure 7. Impellers compared for pump-mix action.

which this power input is obtained, ratio of impeller discharge flow rate to inlet flow rate and head generated by each of them are also tabulated in Table 1. The last column of Table 1 rates the impellers on the basis of head generated by them for equal specific power input ($P/V = 1000$ W/m^3).

From the information contained in the Table 1, the following conclusions can be derived:

1. The highest head number is for BSTRTB, the turbine with the radial trapezoidal blades shrouded on both sides. This is distinctly higher than any other impeller evaluated for pump-mix action. At the same time, the power number for this impeller is the lowest. This makes this impeller the best when different impellers are compared on the basis of equal specific power consumption.

2. Head numbers for open impeller (SBP) and the impeller having blades on both sides of the disk (RT) are very small compared with impellers shrouded on the top or both sides. At the same time, power numbers of these impellers are

Table 1. Comparison of Different Impellers for Pump-Mix Action

Impeller Type	Dimensions	N_P	N_H	N_Q	N	Q_d/Q	h	Rating
SBP	$L = 0.155$, $B = 0.0593$	4.18	0.53	0.61	2.31	27.15	0.035	7
RT	$L = 0.131$, $d = 0.233$	4.86	0.69	0.74	2.19	31.50	0.042	6
TSTRRB	$L = 0.131$	4.07	1.17	0.63	2.33	28.21	0.079	5
TSTNRB	$L = 0.131$, $\beta = 20^\circ$	3.24	1.15	0.69	2.51	33.67	0.091	2
TSTRTB	$L = 0.087$	4.05	1.30	0.63	2.33	28.36	0.088	4
BSTRTB	$L = 0.087$	2.34	2.45	0.28	2.80	14.86	0.240	1
TSTCB	$R = 0.175$, $\alpha = 60^\circ$	3.06	1.10	0.68	2.56	33.50	0.090	3

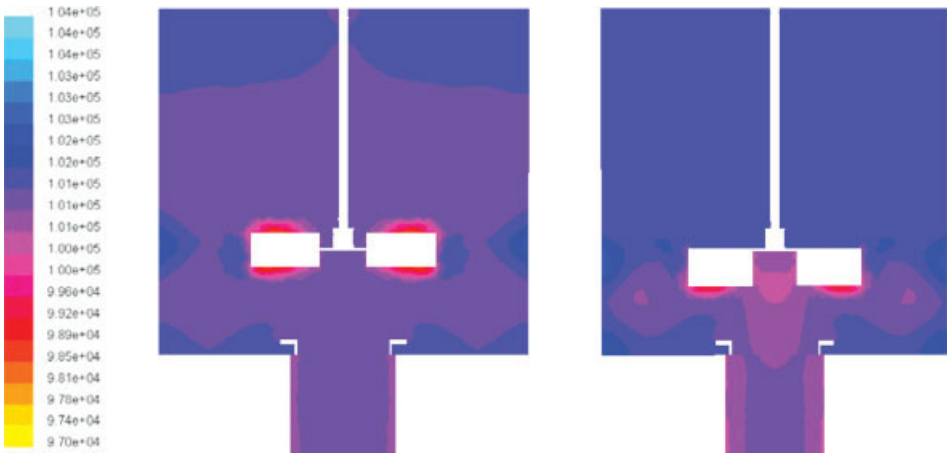

Figure 8. Relative pressure contours in a vertical central plane for RT (left) and TSTRRB (right) at $Q = 0.002222$ m^3/s, $N = 2.5$ s^{-1}.

[Color figure can be viewed in the online issue, which is available at www.interscience.wiley.com.]

higher compared with the other impellers. Because of this, these two impellers fare very poor when compared with the other impellers on the basis of head generated for equal specific power input.

3. Impellers with nonradial blades (TSTNRB and TSTCB) operated in backswept mode fare marginally better than top shrouded impellers with radial blades (TSTRRB and TSTRTB). This is because of smaller power number for the impellers in the former set.

4. The three most efficient impellers based on head generated for a given specific power input are: BSTRTB, TSTNRB, and TSTCB.

Discussion

In the previous section, different impellers have been rated for pump-mix action on the basis of head generated by them for the same specific power input. However, it remains to be seen why different impellers should behave differently when operating at the same speed and handling the same inlet flow rate.

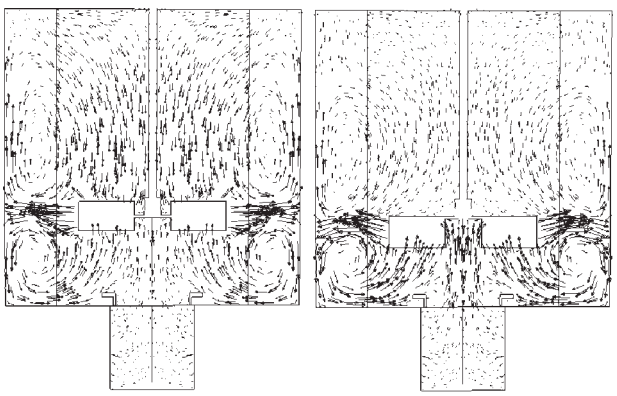

Figure 9. Velocity vectors in a vertical plane for RT (left) and TSTRRB (right) at $Q = 0.002222$ m^3/s, $N = 2.5$ s^{-1}.

Figure 8 shows the contours of the relative pressure (absolute pressure minus the operating pressure with the latter being equal to 101,325 Pa and defined at the outlet) in a vertical central plane of the mixer for RT and TSTRRB. While for RT the low pressure zones can be seen at both the lower and upper edges of the blades, for TSTRRB the low pressure zones can be seen predominantly at the lower edge of the blades. These low pressure zones are responsible for the recirculation loops in the mixer as the liquid leaving the impeller comes back to these low pressure zones after sweeping the tank volume.

Figure 9 shows the velocity vectors in a vertical central plane for RT and TSTRRB at impeller speed of 2.5 s^{-1}. It is clear from the lengths of the vectors that, in case of RT, the presence of low pressure zones at both edges of the blades establishes two almost equally prominent recirculation loops, one above the disk and the other below the disk. On the other hand, in case of TSTRRB only the lower recirculation loop is prominent.

At impeller speed of 2.5 s^{-1}, the impeller discharge flow rate for TSTRRB is computed to be 0.0687 m^3/s whereas the flow rate at the lower suction plane of the impeller is 0.0668 m^3/s. Considering that 0.002222 m^3/s is the feed flow rate, the flow rate attributable to the lower recircualtion loop is 0.0646 m^3/s which is about 94% of the impeller discharge flow rate.

This clearly shows the prominence of the lower recirculation loop over the upper circulation loop in TSTRRB. Similarly for RT, at impeller speed of 2.5 s^{-1}, the impeller discharge flow rate is computed to be about 0.0816 m^3/s whereas the flow rate attributable to the lower recirculation loop is computed to be 0.0377 m^3/s which is about 46% of the impeller discharge flow rate. Therefore, for RT both the recirculation loops are almost equally prominent. The corresponding average velocities at the lower suction plane for RT and TSTRRB are 0.4343 m/s and 0.7253 m/s, respectively. Results from CFD simulations are used to carry out similar calculations for other impellers also. The results are summarized in Table 2 which also lists the average relative pressures at the lower suction plane of the impellers. As can be

Table 2. Some Important Numbers for Different Impellers at $N = 2.5\ s^{-1}$ and $Q = 0.002222\ m^3/s$

Impeller	Q_d (m^3/s)	Q_{lsp} (m^3/s)	Q_{lrl} (m^3/s)	Q_{lrl}/Q_d	A_{lsp} (m^2)	V_{lsp} (m/s)	P_{lsp} (Pa)
SBP	0.0657	0.0160	0.0138	0.21	0.0902	0.1774	49
RT	0.0816	0.0400	0.0377	0.46	0.0921	0.4343	−127
TSTRRB	0.0687	0.0668	0.0646	0.94	0.0921	0.7253	−572
TSTNRB	0.0752	0.0734	0.0712	0.95	0.0921	0.7970	−608
TSTRTB	0.0690	0.0670	0.0648	0.94	0.0934	0.7170	−599
TSTCB	0.0740	0.0718	0.0696	0.94	0.0923	0.7779	−575
BSTRTB	0.0298	0.0287	0.0264	0.89	0.0239	1.2008	−3002

seen from the Table 2 for all the shrouded impellers, the lower recirculation loop is more prominent than the upper circulation loop. For SBP, the upper recirculation loop is more prominent compared with the lower recirculation loop. On the other hand, for RT both the upper and the lower recirculation loops are almost equally prominent. Average velocities at the lower suction plane of RT and SBP are small compared with the top shrouded impellers. This is because of small flow rate in the lower recirculation loop. For BSTRTB, despite of small flow rate in lower recirculation loop, the average velocity at the lower impeller suction plane is the highest because of a small opening in the bottom shroud. Figure 10 shows the relationship between the average velocity at the lower suction plane of the impellers and the average relative pressure at the lower suction plane of the impellers. The trend line shows that to accept the flow coming in at higher velocity the average pressure at the lower suction plane of the impeller should be accordingly smaller. The trend line can alternatively thought of as qualitative observation of principle of conservation of mechanical energy in a highly dissipative system.

Thus from Table 2, it is concluded that despite of the same impeller speed and the same inlet flow rate to the mixer, the average velocities at lower suction plane of the impellers are different because of which the average relative pressures at the lower suction plane of the impellers are different.

Figure 11 shows the path lines traced by the liquid coming into the mixer through the inlet, at impeller speed of 2.5 s^{-1} and flow rate equal to 0.002222 m^3/s, for different

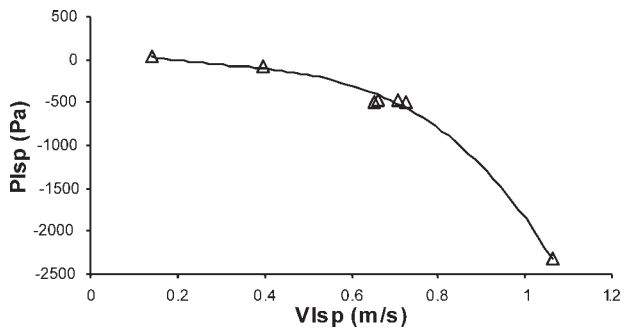

Figure 10. Effect of average velocity on the average relative pressure at the lower suction plane of the impellers at $N = 2.5\ s^{-1}$, $Q = 0.002222\ m^3/s$.

impellers. As can be seen, the incoming liquid directly travels from the suction box to the impeller eye through the lower suction plane of the impeller. As this liquid moves toward the impeller, the flow cross-section available to it gradually reduces as it has to give way to the liquid in the lower circulation loop that is also converging to the lower suction plane of the impeller. Since, in Figure 11, the inlet flow rate and the impeller speed are identical for all the impellers, the different cross-sections of flow paths of the incoming liquid for different impellers indicate that influence of the liquid in the lower recirculation loop on the flow path of the incoming liquid differs from one impeller to other. This can be better understood through the examination of vector plots for SBP, RT, TSTRRB, and BSTRTB as shown in Figure 12. Figure 12 shows that the stream lines of the liquid in the lower recirculation loop, during its way up to the lower suction plane of the impeller, gradually come closer to the centerline thereby gradually reducing the cross-sectional area available to the incoming liquid. In case of SBP, the streamlines of the lower recirculation loop do not come very close to the centerline. Because of this the flow cross-section available for the incoming liquid is large, as shown in Figure 11. The magnitudes of the velocity vectors of the incoming liquid are, accordingly, small. For RT, the streamlines of the liquid in the lower recirculation loop come closer to the centerline than in case of SBP. Therefore, for RT the flow cross-section available to the incoming liquid is smaller than that for SBP, as is evident from Figure 11. For TSTRRB, the proximity of the streamlines of the liquid in the lower recirculation loop to the center line is more than that for RT. The cross-section of the flow path of the incoming liquid is accordingly lesser than that for RT. In case of BSTRTB, owing to the axial discharge from the impeller the streamlines of the liquid in the lower recirculation loop are very close to the centerline right from the suction box. This results into a still smaller flow cross-section available for the incoming liquid. Thus from Figures 11 and 12, it is concluded that the flow pattern of the liquid in the lower recirculation loop affects the cross-section of the flow path leading the incoming liquid to the impeller.

Figures 13 and 14 show the relative pressure profiles along a vertical central line for TSTRRB and RT, respectively. This line completely lies in the flow path of the incoming liquid and therefore shows the representative variation of relative pressure of the incoming liquid as it moves form the suction orifice to the impeller. It is observed that the relative pressure profiles exhibit a minimum, location of which almost coincides with the lower suction plane of the impeller (note that $T = 0.7$ m, $D/T = 0.5$, $C/T = 0.3$, $B/D = 0.2$ and

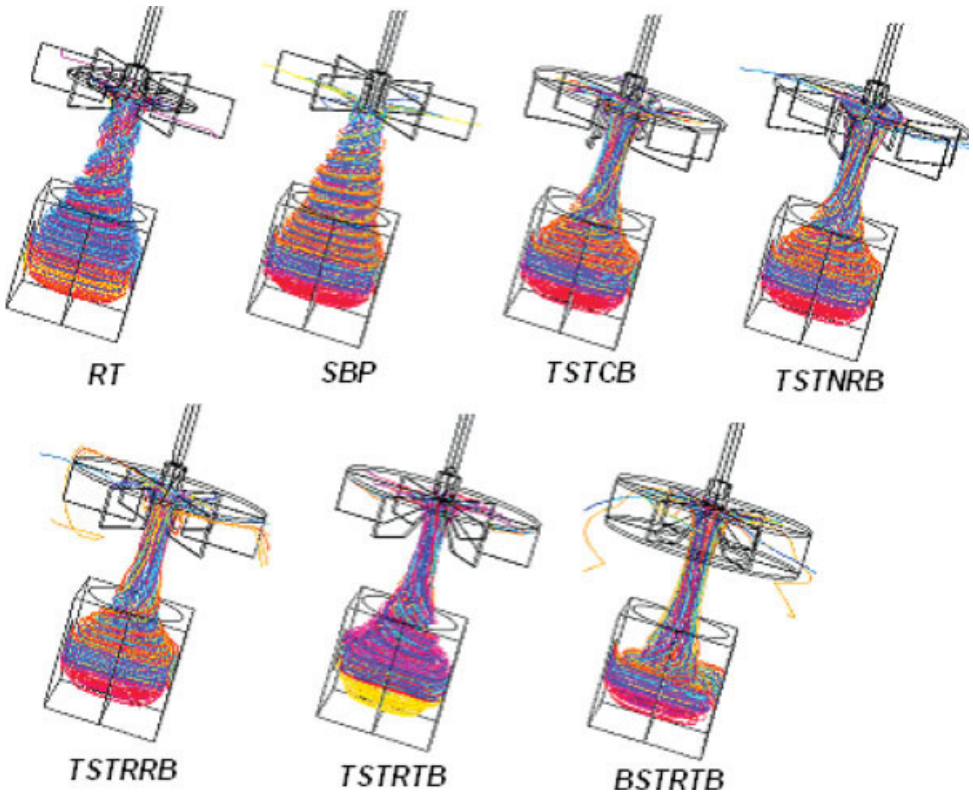

Figure 11. Path lines followed by the liquid entering the mixer through inlet.

[Color figure can be viewed in the online issue, which is available at www.interscience.wiley.com.]

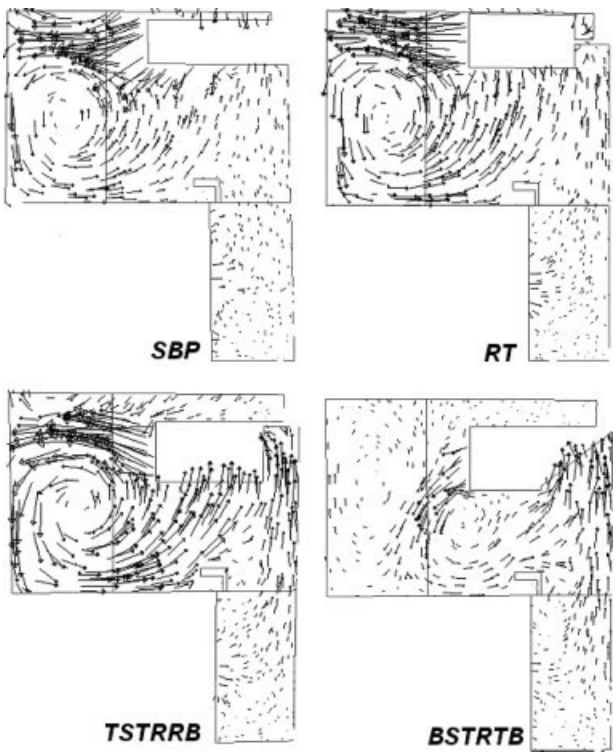

Figure 12. Velocity vectors in a vertical central plane in the vicinity of the impeller at N =2.5 s^{-1}, Q = 0.002222 m^3/s.

with the origin defined at the center of the suction orifice, the axial coordinate of the lower suction plane of the impeller will be 0.14 m).

This pressure minimum seen by the incoming liquid is responsible for its suction by the impeller. With an increase in the impeller speed, the flow rate in the lower recirculation loop and hence the average velocity at the lower suction plane of the impeller also increases. As indicated by the trend line of Figure 10, the average pressure at the lower suction plane of the impeller should, therefore, reduce with an increase in the impeller speed. The minimum pressure along the vertical central line in the flow path of the incoming liquid being nothing but the pressure at the center of the

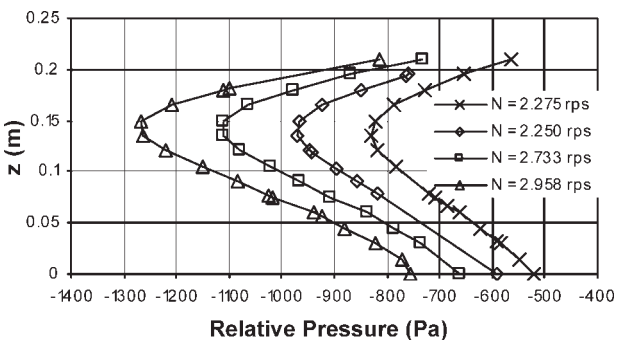

Figure 13. Relative pressure profiles along a vertical central line for TSTRRB for Q = 0.002222 m^3/s.

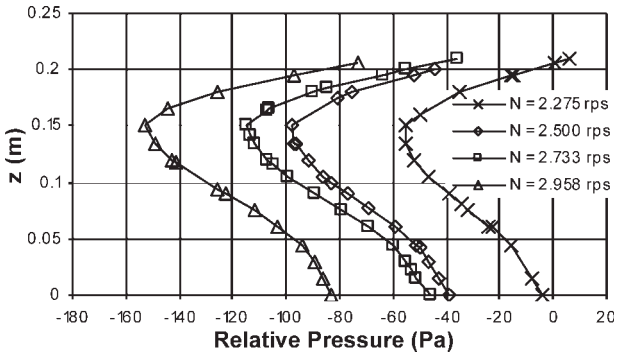

Figure 14. Relative pressure profiles along a vertical central line for RT for $Q = 0.002222$ m^3/s.

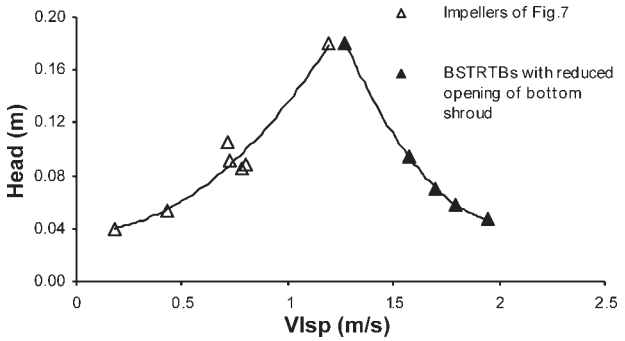

Figure 16. Relationship between the head generated by the impeller and the average velocity at the lower suction plane of the impeller.

lower suction plane of the impeller, the former should follow the trend of the average pressure at the lower suction plane of the impeller and, therefore, should reduce with an increase in the impeller speed. This is indeed shown by Figure 13 and 14. As, for a given impeller speed, the flow rate in the lower recirculation loop is smaller for RT than TSTRRB, values of pressure minimum are larger for RT than TSTRRB.

The pressure at the suction box will be higher than the pressure at the lower suction plane of the impeller both due to converging flow path followed by the incoming liquid and due to pressure drop owing to highly dissipative nature of the turbulent flow. Assuming that the pressure drop along the flow path followed by the incoming liquid does not vary significantly with the impeller type, it can be concluded that the smaller the pressure at the lower suction plane of the impeller, the smaller will be the pressure in the suction box which in turn would mean that the higher will be the head developed by the impeller. This relationship is shown in Figure 15.

Now the trends separately observed in Figures 10 and 15 can be combined to conclude that higher the average velocity at the lower suction plane of the impeller, higher will be the head generated by the impeller. This conclusion is supported by the solid line, passing through the open triangles corresponding to the seven impellers compared for pump-mix action, in Figure 16.

This may lead us to conclude that with increasing average velocity at the lower suction plane of the impeller, the head will continue to rise. However, a closer examination of pressure drop characteristic along the incoming liquid flow path will indicate otherwise. The pressure drop as the incoming liquid is moving from the suction box to the impeller suction plane depends on the cross-section of its flow path. Figure 17 shows the pressure profiles along the vertical central line for SBP, RT, TSTRRB and BSTRTB at 0.002222 m^3/s of inlet flow rate and impeller speed of 2.275 s^{-1}.

As can be seen, for RT and SBP the pressure drop seen by the incoming liquid as it moves from the suction orifice to the impeller suction plane ($z \approx 0.14$ m) is negligible. This is because of a larger flow cross-section available for the incoming liquid, as shown in Figure 11. The pressure drop for TSTRRB is more than that for RT and SBP and is due to a smaller flow cross-section, as seen in Figure 11. On the other hand, pressure drop in case of BSTRTB is much higher and is due to still smaller flow cross-section available for incoming liquid. Consequently, in case of RT and SBP the pressure in the suction box is not much different from the pressure at the lower suction plane of the impeller. On the other hand, in case of BSTRTB the pressure in the suction box is much higher compared with the pressure at the lower suction plane of the impeller. On further reducing the opening in the bottom shroud of BSTRTB, though the pressure at

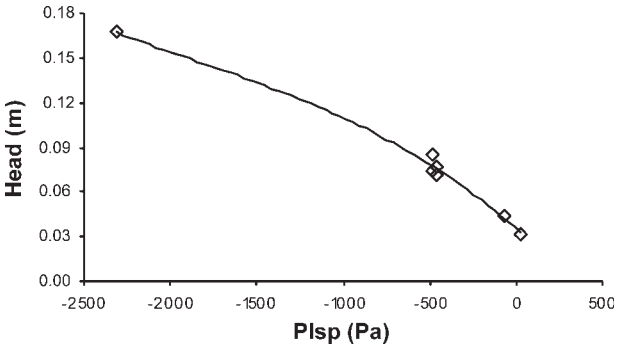

Figure 15. Relationship between the head generated by the impeller and the average relative pressure at the lower suction plane of the impeller at $N = 2.5$ s^{-1}, $Q = 0.002222$ m^3/s.

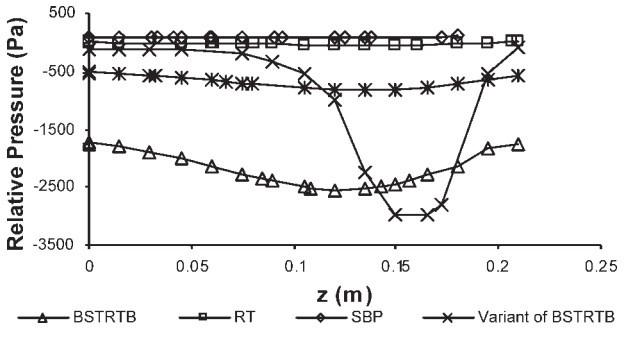

Figure 17. Relative pressure profiles along a vertical central line for BSTRTB, RT, SBP, TSTRRB and a variant of BSTRTB at $Q = 0.002222$ m^3/s and $N = 2.275$ s^{-1}.

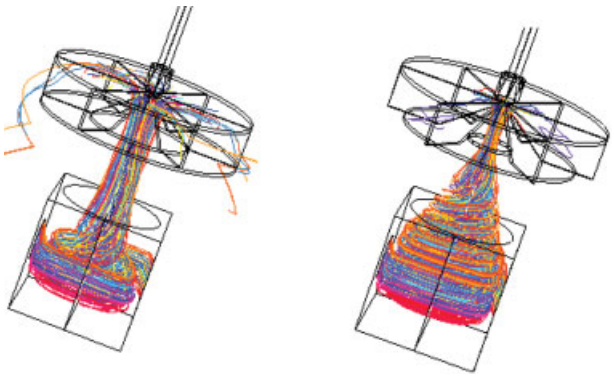

Figure 18. Path lines traced by the inlet fluid for BSTRTB (left) and a variant of BSTRTB (right) at Q = 0.002222 m^3/s and N = 2.275 s^{-1}.

[Color figure can be viewed in the online issue, which is available at www.interscience.wiley.com.]

the lower suction plane of the impeller will reduce, depending on the flow cross-section of the incoming liquid, the pressure drop along the flow path of the incoming liquid and hence the pressure in the suction box may increase and, therefore, the head may reduce. This behavior exhibited by a variant of BSTRTB is shown in Figure 17. In this variant of BSTRTB, the outer and inner diameters of the bottom shroud are 0.10 m less than that in BSTRTB. As can be seen, reduction of the diameter of the central opening in bottom shroud does reduce the pressure seen by the incoming liquid at the lower suction plane of the impeller. However, the pressure drop along the flow path of the incoming liquid for this variant of BSTRTB is much higher than that for BSTRTB. As a result, the pressure in the suction box for the variant of BSTRTB is much higher compared to the BSTRTB. This pressure is only slightly less than that for RT and SBP and hence the head produced by this variant of BSTRTB is similar to that produced by RT and SBP despite of a very small pressure at the lower suction plane of the impeller. Figure 17 shows that for variant of BSTRTB, most of the pressure drop occurs in the vicinity of the impeller suction plane. This is well-corroborated by the path lines shown in Figure 18 which shows that the cross-section of the incoming liquid flow path, though large elsewhere, becomes very small near the impeller suction plane.

Thus if further experiments are done with gradual reduction in the opening of the bottom shroud and the resulting data are included in Figure 16, one should eventually observe the head to reduce with increasing average velocity at lower suction plane of the impeller. To confirm this, five more CFD simulations were carried out with reducing bottom shroud opening radius (0.0825, 0.0775, 0.0675, 0.0575 and 0.0475 m compared with 0.0875 m for BSTRTB). The results are plotted in Figure 16 as solid triangles. Trend line through them, indeed suggests that beyond a certain value of the average velocity at the impeller suction, head tends to reduce. On further reduction in the bottom shrouded opening a stage may reach when the impeller may not pump at all and ceases to be a pump-mix impeller. This clearly makes the opening in the bottom shroud of the BSTRTB an optimization variable.

Thus we see that the head developed by an impeller depends on the interaction between the liquid in the lower recirculation loop and the incoming liquid. The liquid in the lower recirculation loop affects the head by influencing both the pressure at the lower suction plane of the impeller and the pressure drop along the flow path of the incoming liquid. While the pressure at the lower suction plane of the impeller

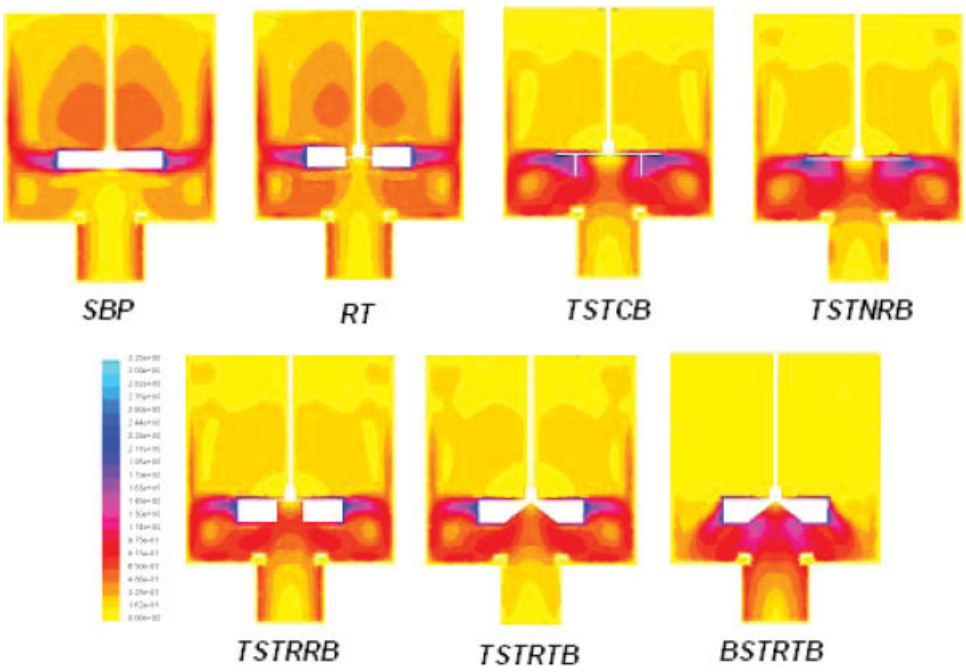

Figure 19. Velocity contours in a vertical central plane for Q = 0.002222 m^3/s and N = 2.275 s^{-1}.

[Color figure can be viewed in the online issue, which is available at www.interscience.wiley.com.]

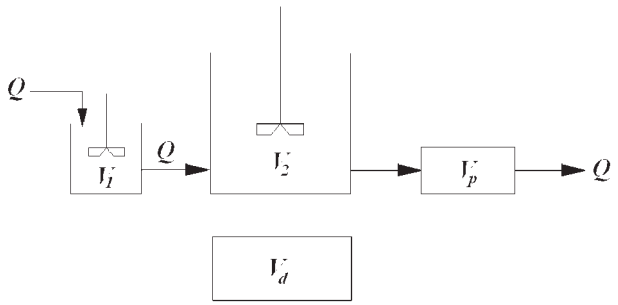

Figure 20. The compartment model.

can be varied by varying the average velocity at the lower suction plane of the impeller (by varying the area of the impeller suction plane), it is difficult to control the effect of lower recirculation loop on the flow path of the incoming liquid. However, effect of lower recirculation loop on the flow path of the incoming liquid can be almost completely eliminated by using a draft tube that runs from the suction box to just below the lower suction plane of the impeller and hence ensures a physical separation between the lower recirculation loop and the flow path of the incoming liquid.

The two important facts observed in the previous section can now be explained. It was observed that head generated by the open impeller (SBP) and disk impeller having blades on both sides of the disk (RT) are smaller compared to the top shrouded impellers (TSTRRB, TSTRTB, TSTCB, TSTNRB). Similarly it was observed that the impeller shrouded on both sides (BSTRTB) gives a very high head compared with other impellers evaluated in this study. Both of these observations stand explained in the light of the second last column of the Table 2 and solid trend line of Figure 16.

Design Modifications

Figure 19 shows the velocity contours in a vertical central plane for different impellers at $Q = 0.002222$ m^3/s and $N = 2.275$ s^{-1}. As can be seen, for top shrouded impellers the velocities in a significant portion of the region above the impeller are small. For BSTRTB this problem is more pronounced, as the velocities in the whole region above the impeller are very small. This can be attributed to the axial discharge from the impeller, as seen in Figure 12 and a very small flow number (0.2751).

Because of very small velocities in the whole region above the impeller, poorly mixed regions and dead regions are likely to be present in the tank employing BSTRTB. The quantitative estimate of this can be obtained by the compartment modeling using the CFD predicted exit age distribution curves. This approach has earlier been used for compartment

Table 3. Summary of Compartment Modeling at $N = 2.275$ s^{-1}, $Q = 0.002222$ m^3/s

Impeller	% V_p	% V_1	% V_2	% V_d
RT	0.91	3.40	95.51	0.18
TSTCB	0.50	1.90	97.20	0.40
BSTRTB	5.43	1.40	77.96	15.21
Design-1	*1.63*	*4.00*	*94.21*	*0.17*
Design-2	*0.51*	*4.50*	*94.91*	*0.09*

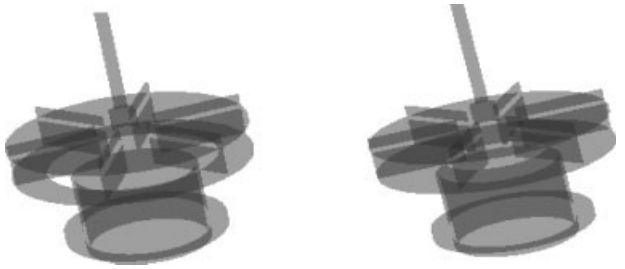

Figure 21. Two new designs of pump-mix impellers.

modeling of a bench-scale pump-mixer.[24] Similar approach has been used here to quantify the goodness of flow field produced by BSTRTB. The details of obtaining the CFD predicted virtual exit age distribution curves and fitting the compartment model are omitted here for brevity. Among the different compartment models that were tried, the one with a plug flow vessel in series with two perfectly mixed vessels and a dead volume was found to be the best. The model is shown in the Figure 20. The first small mixed vessel of this model represents the volume occupied by the incoming liquid between the suction box and the impeller eye.[24] The plug flow volume represents the volume of the vessel close to the outlet which is not swept by the upper recirculation loop. The dead volume corresponds to the corners of the vessel that are not penetrated by the liquid in the recirculation loops and the second perfectly mixed vessel represents the remaining volume. Table 3 gives the percentage of these volumes for RT, TSTCB, and BSTRTB for $N = 2.275$ s^{-1} and $Q = 0.002222$ m^3/s, as obtained by fitting the exit age distribution of the compartment model into the exit age distribution curve predicted by CFD simulations.[24] As can be seen, the contributions of plug flow vessel and dead volume are substantial for BSTRTB. Both of these volumes are undesirable from mixing point of view.

It is generally accepted that in liquid–liquid dispersions in mechanically agitated vessels, the breakage of drop predominantly occurs in the impeller region. The fine drops produced here move through the tank along the recirculation loops during which they undergo coalescence and grow in size before they come back to the impeller and are broken again.[37] If the circulation frequency of the drops is large compared with coalescence frequency of the drops, the dispersion will be homogeneous as the drops leaving the impeller will not get sufficient time to undergo repeated coalescence before they are brought back to the impeller. On the contrary, if the circulation frequency is less than the coalescence frequency, dispersion will not be homogeneous.[38] The interfacial area in the latter case will be much less than the former case.

Though, for the top shrouded impellers, the compartment modeling does not show presence of poorly mixed or dead volumes, from the fifth column of Table 2, it is evident that

Table 4. Evaluation of New Designs of the Pump-Mix Impellers

Impeller Type	N_P	N_H	N_Q	N	Q_d/Q	h
Design-1	3.8554	2.0424	0.5516	2.371	25.23	0.143
Design-2	2.7215	3.1255	0.3246	2.662	16.67	0.277
BSTRTB	2.3406	2.4480	0.2751	2.800	14.86	0.239

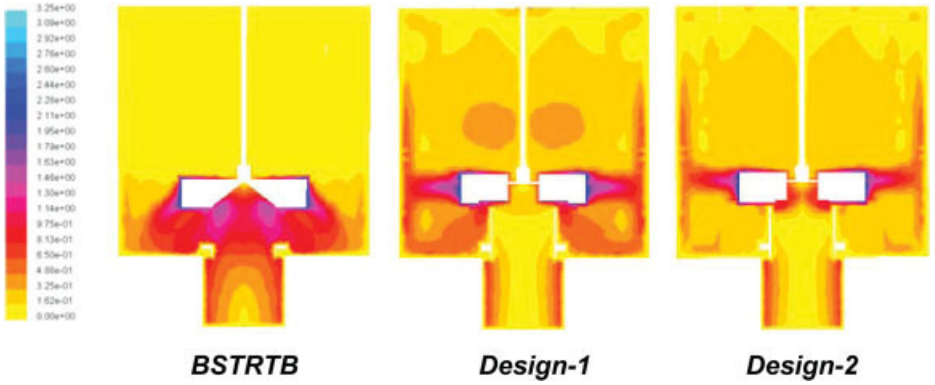

Figure 22. Velocity contours in a vertical plane for BSTRTB and two new designs at $N = 2.275\ s^{-1}$, $Q = 0.002222\ m^3/s$.

[Color figure can be viewed in the online issue, which is available at www.interscience.wiley.com.]

the recirculation rates for the region above the top shrouded impellers are much smaller. Consequently, if employed for creating liquid–liquid dispersions, the specific interfacial area produced by a top shrouded impeller is expected to be smaller than an open impeller or an impeller having blades on both sides of the disk which have good recirculation both above and below the impeller. For this reason, an impeller giving high recirculation rate both above and below the impeller is better than the impeller giving high recirculation rate only below the impeller. Thus a good pump-mix impeller should satisfy the following requirements:

1. Should be able to give high head for a given specific power input
2. Should generate a flow field devoid of poorly mixed zones and dead zones
3. Should generate good recirculation both above and below the impeller

Among the impellers compared here, while the open impeller (SBP) and impeller having blades on both sides of the disk (RT) satisfy the second and third requirements, they fail to satisfy the first requirement, the basic requirement to be satisfied by an impeller to be employed for pump-mix action. On the other hand, the BSTRTB satisfies the first requirement of high head but does not satisfy the second and third requirements. The top shrouded impellers, on the other hand, partially satisfy the first requirement, satisfy the second requirement but do not satisfy the last requirement.

Since none of the impeller evaluated here satisfies all the requirements, it is important to modify one of them, using the insight gained in the previous section, to conceptualize a new design of the impeller that along with generating a high head for a given specific power input should also give good flow field devoid of poorly mixed and dead region and ensure good recirculation both above and below the impeller. In this study, the TSTRRB is chosen for design modifications.

Both for RT and TSTRRB, blades are identical but while for RT the recirculation is good both above and below the impeller, because of absence of blades above the disk in TSTRRB, the recirculation is poor above the impeller. Clearly the redistribution of a fraction of blade area of TSTRRB from below the disk to above the disk should improve the recirculation in the region above the impeller. However, the head developed by this impeller will be lower than TSTRRB because of reduced lower recirculation flow rate and hence reduced average velocity at the lower suction plane of the impeller. From the discussion in the previous section, it can be concluded that a high head should be obtained when the average velocity at the lower suction plane of the impeller is high and the cross-section of the flow path of the incoming liquid is also large. While, provision of a bottom shroud should ensure high average velocity at the lower suction plane of the impeller, provision of a draft tube from suction box to just below the lower suction plane of the impeller should ensure a large cross-section for the flow path of the incoming liquid. Based on this idea, two new designs of pump-mix impeller are evaluated. In both of them blade width above the disk is about 29% (0.02 m of 0.07 m of total width) of the total blade width. Whereas, in the first design the width of the bottom shroud is 0.05 m, in the second design width of the bottom shroud is 0.10 m. Both the designs have a draft tube extending from the suction box to just below the lower suction plane of the impeller. The designs are shown in Figure 21.

CFD simulations are carried out for the two designs and the resulting characteristics are compiled in Table 4. Data for BSTRTB are also given for comparison. N, Q_d/Q, and h are the impeller speed, ratio of impeller discharge flow rate to inlet flow rate, and head generated by the impeller for a given specific power input ($P/V = 1000\ W/m^3$).

Figure 22 shows the velocity contours for BSTRTB and the two proposed designs. As can be observed, the velocity

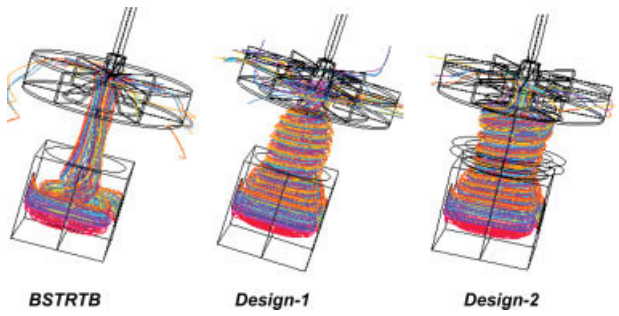

Figure 23. Path lines of incoming liquid for BSTRTB and two new designs at $N = 2.275\ s^{-1}$, $Q = 0.002222\ m^3/s$.

[Color figure can be viewed in the online issue, which is available at www.interscience.wiley.com.]

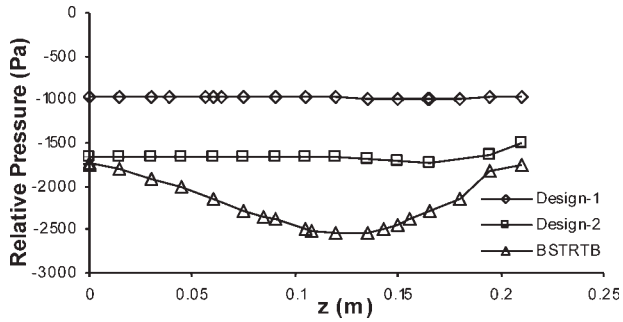

Figure 24. Pressure profiles along a vertical central line for BSTRTB and two new designs at $Q = 0.002222$ m^3/s and $N = 2.275$ s^{-1}.

fields produced by both the modified designs are more homogeneous than that produced by BSTRRB. The head generated by Design-2 at equal specific power input, ($P/V = 1000$ W/m^3) is more than even BSTRTB. Its flow number, though small, is also more than that of BSTRTB. Design-1 on the other hand gives a higher flow number which comes at the cost of reduced head. However, the head produced by the Design-1 is still much more than the other top shrouded impellers compared in the previous section. For systems having low coalescence tendency (systems with small interfacial tension), Design-2, having lower flow number and higher head number can be used. On the other hand, for systems having high coalescence tendency (systems with high interfacial tension) Design-1 having higher flow number should be preferred.

Figure 23 shows the path lines of the incoming liquid for BSTRRB and the new designs. The effect of the isolation of flow path of incoming liquid from the liquid in the lower recirculation loop due to draft tube is clearly visible. Figure 24 shows the pressure profiles along the vertical central line. In both the designs, owing to large cross-sectional area of the flow path of the incoming liquid, the pressure drop from the suction box to the impeller eye is negligible. This helps realize the low pressure at the lower suction plane of the impeller at the suction box which manifests in higher head.

Compartment modeling of the two designs was also carried out. The results are compiled in the last two rows of Table 3. Comparison with BSTRTB shows that the new designs effectively eliminate the plug flow and dead regions. The higher value of percentage contribution of the first mixed vessel is attributable to the enhancement of volume occupied by incoming liquid between suction box and impeller because of the presence of the draft tube. The values of Q_{lrl}/Q_d were also computed and were found to be 0.56 and 0.31, respectively, for Design-1 and Design-2. This indicates that the impeller discharge flow rate is distributed well both above and below the impeller. Thus, both the new designs satisfy the three requirements, mentioned earlier, to be satisfied by a pump-mix impeller.

Conclusions

CFD simulations for TSTNRB operated in backswept mode have been carried out and validated using experimental data. Following the extensive validation that has been done in two previous studies[23,24] and in the present study, CFD has been applied to simulate pump-mix action of different impellers. These impellers have been compared for a give inlet flow rate (0.002222 m^3/s) under the same geometric setting ($C/T = 0.3$, $D = T/2$, equal blade area). The important dimensionless numbers required to characterize the pump-mix action have been tabulated. The impellers have been rated on the basis of the head generated by them for a given specific power input (1000 W/m^3). The turbine with trapezoidal blades shrouded on both sides (BSTRTB) was found to be the best. Straight blade paddle (SBP), an open impeller and Rushton turbine (RT), an impeller with blades present on both sides of the disk were found to fare poor. An attempt has been made to understand as to why different impellers rotating at same speed and handling the same inlet flow rate to the mixer give different head. Based on this insight, two new designs of the impellers that are expected to meet the requirements to be satisfied by an impeller when used in a pump-mix mixer settler are proposed.

Notation

a = constant specifying lower limit of specific power input, kg/m/s^3
b = constant specifying upper limit of specific power input, kg/m/s^3
A_{lsp} = area of the lower suction plane of the impeller, m^2
B = impeller blade width, m
L = Impeller blade length, m
C = impeller off bottom clearance, m
d = disk diameter for Rushton turbine, m
D = impeller diameter, m
g = acceleration due to gravity, m/s^2
h = head generated by the impeller, m
h_r = required head of light phase, m
H = tank height, m
H_l = height of light phase recycle pipe line, m
H_m = height of over flow level in mixer plus suction box, m
N = impeller speed, 1/s
N_H = head number
N_P = power number
N_Q = flow or pumping number
P = power consumption, kg m^2/s^3
P_{lsp} = average relative pressure at the lower suction plane of the impeller, kg/m/s^2
Q = volumetric flow rate, m^3/h
Q_d = impeller discharge flow rate, m^3/s
Q_{lrl} = flow rate in the lower recirculation loop of the impeller, m^3/s
Q_{lsp} = flow rate at the lower suction plane of the impeller, m^3/s
R = radius of curvature of blades in top shrouded impeller with curved blades, m
T = tank diameter, m
V = volume of the mixer, m^3
V_1 = volume of the first perfectly mixed vessel of the compartment model, m^3
V_2 = volume of the second perfectly mixed vessel of the compartment model, m^3
V_d = volume of the dead region of the compartment model, m^3
V_{lsp} = average velocity at the lower suction plane of the impeller, m/s
V_p = volume of the plug flow vessel of the compartment model, m^3

Greek letters

β = angle between the line joining blade tip to the center and the blade for TSTNRB
ε = specific turbulence energy dissipation rate, m^2/s^3
ρ = density, kg/m^3
ρ_l = density of light phase, kg/m^3
ρ_m = density of mixed phase, kg/m^3

Abbreviations

CFD = computational fluid dynamics
SBP = straight blade paddle
RT = Rushton turbine
TSTRRB = top shrouded turbine with radial rectangular blades
TSTNRB = top shrouded turbine with nonradial rectangular blades
TSTRTB = top shrouded turbine with radial trapezoidal blades
BSTRTB = both side shrouded turbine with radial trapezoidal blades
TSTCB = top shrouded turbine with curved blade

Literature Cited

1. Coplan BV, Davidson JK, Zebroski EL. The pump-mix mixer settler, a new liquid-liquid extractor. *Chem Eng Prog*. 1954;15(8):403.
2. Lott JB, Warwick GI, Scuffham JB. Design of large scale mixer-settlers. *Trans Soc Mining Engineers*. 1972;252:27–35.
3. Bates RL, Fondy PL, Corpstein RR. An examination of some geometric parameters of impeller power. *Ind Eng Chem Process Design Dev*. 1963;2(4):310.
4. Gray DJ, Treybal RE, Barnett SM. Mixing of single and two phase systems: power consumption of impellers. *AIChE J*. 1982;28(2): 1995–1999.
5. Placek J, Tavlarides LL. Turbulent flow in stirred tanks. I. Turbulent flow in the turbine impeller region. *AIChE J*. 1985;31(7):1113–1120.
6. Placek J, Tavlarides LL, Smith GW, Fort I. Turbulent flow in stirred tanks. II. A two-scale model of turbulence. *AIChE J*. 1986;32(11): 1771–1786.
7. Mahoust M, Cognet G, David R. Two component LDV measurements in a stirred tank. *AIChE J*. 1989;35(11):1770–1778.
8. Kresta SM, Woods PE. Prediction of three-dimensional turbulent flow in stirred tanks. *AIChE J*. 1991;37(3):448–460.
9. Harvey AD, Lee CK, Rogers SE. Steady state modeling and experimental measurements of a baffled impeller stirred tank. *AIChE J*. 1995;41(10):2177–2186.
10. Zhou G, Kresta SM. Impact of tank geometry on the maximum turbulence energy dissipation rate for impellers. *AIChE J*. 1996; 42(9):2476–2490.
11. Rutherford K, Lee KC, Mahmoudi SMS, Yianneskis M. Hydrodynamic characteristics of dual Rushton impeller stirred vessels. *AIChE J*. 1996;42(2):332–346.
12. Harvey AD, Rogers SE. Steady and unsteady computation of impeller stirred reactor. *AIChE J*. 1996;42(10):2701–2712.
13. Armenante PM, Chou CC. Velocity profiles in a baffled vessel with single or double pitch-blade turbines. *AIChE J*. 1996;42(1):52–54.
14. Brucato A, Ciofalo M, Grisafi F, Micale G. Numerical prediction of flow fields in baffled stirred vessels: a comparison of alternative modeling approaches. *Chem Eng Sci*. 1998;53(21):3653.
15. Lee KC, Yianneskis M. Turbulence properties of the impeller stream of a Rushton turbine. *AIChE J*. 1998;44(1):13–24.
16. Schafer M, Yianeskis M, Wachter P, Durst F. Trailing vortices around a 45° pitched-blade impeller. *AIChE J*. 1998;44(6):1233–1246.
17. Micale G, Brucato A, Grisafi F, Ciofalo M. Prediction of flow fields in a dual impeller stirred vessel. *AIChE J*. 1999;45(3):445–464.
18. Jos D, Vanden Akker HEA. Large eddy simulations of the flow driven by a Rushton turbine. *AIChE J*. 1999;45(2):209–221.
19. Wu J, Pullum L. Performance analysis of axial-flow mixing impeller. *AIChE J*. 2000;46(3):489–498.
20. Sharp KV, Adrian RJ. PIV study of small-scale flow structure around a Rushton turbine. *AIChE J*. 2001;47(4):766–778.
21. Aubin J, Fletcher DF, Xuereb C. Modeling of turbulent flow in stirred tanks with CFD: the influence of modeling approach, turbulence model and numerical scheme. *Exp Thermal Fluid Sci*. 2004; 28(5):431.
22. Li M, White G, Wilkinson D, Roberts KJ. Scale up study of retreat curve impeller stirred tanks using LDA measurements and CFD simulations. *Chem Eng J*. 2005;108(1/2):81.
23. Singh KK, Mahajani SM, Shenoy KT, Patwardhan AW, Ghosh, SK. CFD modeling of pilot-scale pump-mixer: single phase head and power characteristics. *Chem Eng Sci*. 2007;62:1308.
24. Singh KK, Mahajani SM, Shenoy KT, Ghosh SK. Computational fluid dynamics modeling of bench-scale pump-mixer: head, power and residence time distribution. *Ind Eng Chem Res*. 2007; 46(7):2180–2190.
25. Harel G, Kogan M, Meyer D, Semiat R. Mass transfer in the IMI turbine pump-mixer. *Proceedings of International Solvent Extraction Conference (ISEC-1983)*, 1983; 76.
26. Rao NVR, Baird MHI. McKee combined mixer settler: some laboratory studies. *Can J Chem Eng*. 1984;62:497.
27. Singh KK, Shenoy KT, Ghosh SK. Neural network modeling of single phase head and power characteristics of a pump-mixer using top shrouded Rushton turbine impeller. *Proceedings of CHEMCON-2003*, 19–22 Dec, Bhubneswar, India.
28. Singh KK, Shenoy KT, Mahendra AK, Ghosh SK. Artificial neural network based modeling of head and power characteristics of pump-mixer. *Chem Eng Sci*. 2004;59:2937.
29. Lo TC, Baird MHI, Hanson C. *Handbook of Solvent Extraction*. New York: Wiley, 1983.
30. Godfrey JG, Slater MJ. *Liquid-Liquid Extraction Equipment*. New York: Wiley, 1994.
31. Treybal RE. *Mass Transfer Operations*. Singapore: McGraw-Hill, 1980.
32. Alopaeus V, Koskinen J, Keskinen KI. Simulation of the population balances for liquid-liquid systems in a nonidela stirred tank, Part 1: Description and qualitative validation of the model. *Chem Eng Sci*. 1999;54:5887.
33. Maggioris D, Goulas A, Alexopoulos AH, Chatzi EG, Kiarissides C. Prediction of particle size distribution in suspension polymerization reactors: effect of turbulence non homogeneity. *Chem Eng Sci*. 2000;55:4611.
34. Alexopoulos, RH, Maggirois D, Kiparissides C. CFD analysis of turbulence homogeneity in mixing vessel. A two compartment model. *Chem Eng Sci*. 2002;57:1735.
35. Alopaeus V, Koskinen J, Keskinen KI, Majander J. Simulation of the population balances for liquid-liquid systems in a nonideal stirred tank, Part 2: Parameter fitting and the use of the multiblaock model for dense dispersions. *Chem Eng Sci*. 2002;57:1815.
36. Shekhar SM, Jayanti S. CFD study of power and mixing time for paddle mixing in unbaffled vessels. *Trans IChemE*. 2002;80(A):482.
37. Kumar S, Kumar R, Gandhi KS. A multi-stage model for drop breakage in stirred vessels. *Chem Eng Sci*. 1992;47(5):971.
38. Coulaloglou CA, Tavlarides, LL. Drop size distributions and coalescence frequencies of liquid-liquid dispersions in flow vessels. *Chem Eng Sci*. 1976;22(2):289.

Manuscript received Apr. 18, 2007, and revision received Sept. 21, 2007.